Grant Agreement no. 226967
Seismic Hazard Harmonization in Europe
Project Acronym: SHARE

SP 1-Cooperation

Collaborative project: Small or medium-scale focused research project

THEME 6: Environment

Call: ENV.2008.1.3.1.1 Development of a common methodology and tools to evaluate earthquake hazard in Europe

D2.3 – Calibration of Seismic Design Codes using Loss Estimation

Due date of deliverable: 31.05.2011
Actual submission date: 11.09.2001

Start date of project: 2009-06-01 Duration: 36

University of Pavia (UPAV)

Helen Crowley, Vitor Silva, Ihsan Engin Bal, Rui Pinho

Revision: 1

Dissemination Level		
PU	Public	x
PP	Restricted to other programme participants (including the Commission Services)	
RE	Restricted to a group specified by the consortium (including the Commission Services)	
CO	Confidential, only for members of the consortium (including the Commission Services)	

TABLE OF CONTENTS

LIST OF FIGURES

LIST OF TABLES

1. INTRODUCTION

1.1. Performance-Based Seismic Design

Seismic design codes for the earthquake-resistant design of structures are fundamental for the mitigation of seismic risk. Codes provide guidance for engineers (who may not have specialist training in earthquake engineering) on analysing the effects of earthquake ground motions on structures, and on the required configuration and detailing for improved seismic performance. The crucial elements of a design code are the definition of the seismic actions to be considered in the design and the minimum levels of force and displacement that the structure should achieve under the imposed actions.

The basic performance objective in most seismic design codes has always been related to ensuring the life safety of the building occupants, generally through collapse prevention. The ground motions for which life safety was to be ensured by the design, at least until recently, have been based on the same criterion in almost every seismic design code throughout the world: the 5%-damped spectral acceleration with a return period of 475 years (Bommer and Pinho, 2006).

The experience of the 1994 Northridge earthquake and the 1995 Great Hanshin [Kobe] earthquake demonstrated that both economic losses and human casualties could be considerable, even if the no-collapse objective had been met for many structures (Bommer and Pinho, 2006). Performance-based seismic design (PBSD) formalises the approach of citing multiple objectives for structures to withstand minor or more frequent levels of shaking with only non-structural damage, whilst also ensuring life safety and no-collapse under severe shaking (ATC, 1978) (Figure 1.1).

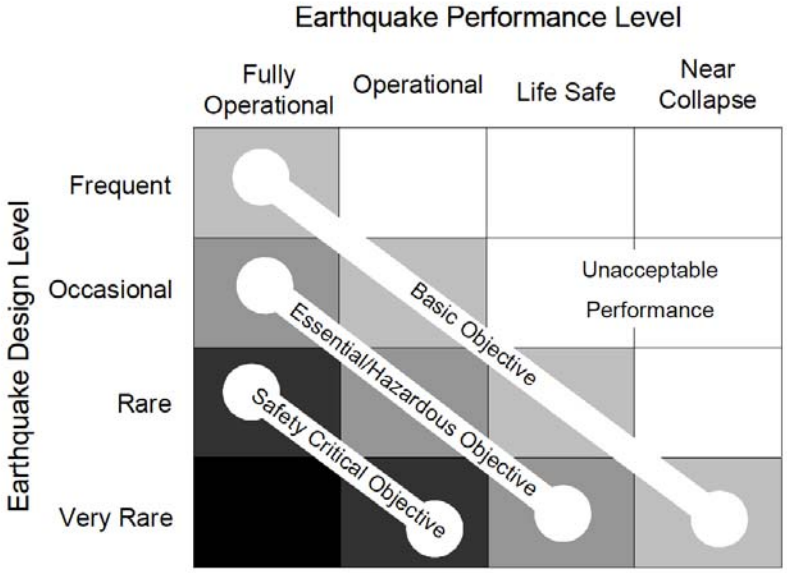

Figure 1.1 Couples of seismic loading and performance in the framework of Vision 2000 (adapted from SEAOC, 1995).

These objectives define the limit states, which describe the maximum extent of damage expected to the structure for a given level of ground motion. Many seismic codes define limit states or performance objectives according to the return period (TR) (or probability of exceedance, PR) of a given level of ground motion. In EN 1998, two requirements are cited: 1) “no-collapse” (recommended TR = 475 years) and 2) “damage limitation” (TR = 95 years).

In many seismic design codes, performance-based requirements are implemented explicitly on the basis of return period. On others, serviceability and operational objectives may be assumed implicit, and are not necessarily afforded an explicit return period. Despite the diversity of definitions of different limit states, there is clear persistence in the adoption of 475 years as a basis for “life safety”, although several codes have recently begun to adopt 2475 years as the return period for the no-collapse criterion, albeit subsequently rescaled to incorporate an assumed inherent margin of safety against collapse (e.g. NEHRP, 2003).

1.2. Risk-Based Approach to Design

The 2009 revision to the NEHRP Provisions introduces a new conceptual approach to the definition of the input seismic action (NEHRP, 2009). The seismic input (maximum considered earthquake) is modified by a risk coefficient (for both short and long periods). This coefficient is derived from a probabilistic formulation of the likelihood of collapse (Luco *et al*., 2007). These modifications change the definition of seismic input to that which ensures a more uniform level of collapse prevention. SHARE Deliverable 2.2 (Weatherill *et al*., 2010) describes in more detail this method.

The risk-targeted approach presented by Luco *et al.* (2007) only considers the no-collapse limit state. It remains to be seen how this can be adapted to consider serviceability and damage limitation requirements. The degree of seismic detailing required to meet performance based objectives is affected by the behaviour of the structure at lower intensities. A longer term objective for performance based seismic design may be to consider the relative cost-benefit that a given level of detailing produces. Such an approach has been proposed by Bommer *et al*. (2005), who describe an iterative procedure to determine the cost versus benefit using displacement-based earthquake loss assessment. This approach would allow for designers to consider losses at other limit states besides collapse.

This deliverable extends the paradigm shift proposed by Bommer *et al*. (2005) for the calibration of design codes, and applies it to a case study application in Turkey.

2. CODE CALIBRATION USING LOSS ASSESSMENT

2.1. Introduction

The basic principle of the proposal made herein for the calibration of codes for performance-based design is that the matching of seismic loading and performance levels should be based on a quantitative comparison of the incremental costs of adding seismic resistance and of the associated losses that can thus be avoided. Such as cost-benefit approach to code calibration requires that the structural parameters in the vulnerability model can easily be adapted to model increasing levels of seismic resistance, and thus enhanced design criteria. The decisions regarding investment in engineering design to achieve specified levels of seismic resistance, whilst informed by engineering seismologists and earthquake engineers, must ultimately reside with owners and regulators.

The procedure proposed herein has similar components to a methodology under development at the PEER Centre (e.g. Porter, 2003) for PBSD: the loss in terms of costs, casualties and downtime is considered for increasing levels of hazard from a cost-benefit viewpoint in order to define the loading-performance couple used in the design. However, an important difference between the method proposed herein and that by PEER is that the latter has not been derived for the calibration of design codes. The PEER approach is applicable for building-specific design and thus does not consider the convolution of hazard and vulnerability **on an urban scale**, which is the basis of the methodology proposed herein.

2.2. Iterative Loss Modelling for Different Seismic Design Levels.

The first step in the proposed framework requires the building stock that will be located within a given area of interest to be modelled in terms of the number and location of different construction types and of different numbers of storeys, i.e. as building classes.

The next stage is to assign to each building class different levels of earthquake resistance through increments in stiffness/ductility over and above those resulting from non-seismic design according to the relevant building regulations. The DBELA procedure, described in Chapter A2 is used herein; since it is based on the mechanical properties of structures, it is well suited to modelling an incremental improvement of the design levels. The basic level of non-seismic design defined by the relevant building codes is design level SC_1, and each incremental improvement represents another SC_k.

Each level of building stock resistance is then subjected to the model of the seismic hazard in order to estimate the mean damage ratio (MDR) at different annual frequencies of exceedance (AFOE) for each location in the area under consideration. The most rigorous approach to produce loss curves of MDR versus AFOE is through an event-based method, as described in Appendix A. Loss

(MDR) exceedance curves for various levels of seismic resistance for a given construction type, as presented in Figure 2.1, can in this way be constructed. It should be appreciated that Figure 2.1 is illustrative and in practice a much larger number of SC_k levels is envisaged for actual code calibration studies.

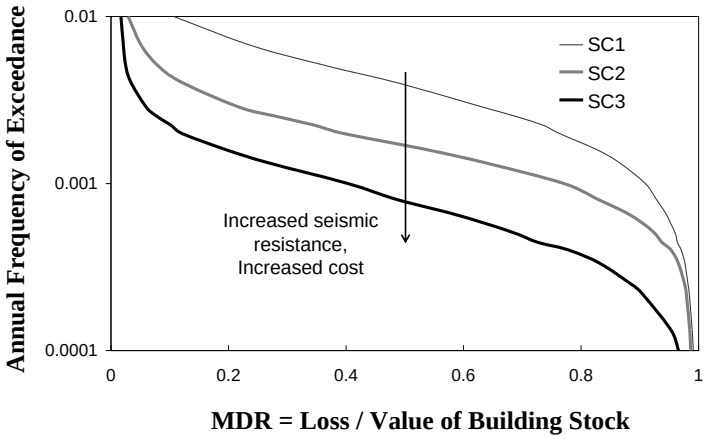

Figure 2.1 Illustrative plots of mean damage ratio versus annual frequency of exceedance for different levels of seismic resistance (SC_k) for one construction type.

2.3. Cost-benefit Basis for the Optimum Seismic Resistance.

The next part of the process requires the decision makers to choose the level of seismic protection that a society is willing to pay for. There are a number of ways in which the cost-benefit of each SC_k can be presented. The simplest way of determining the optimum seismic resistance (in terms of the balance between investment and losses avoided) could be to look at a single scenario, such as the repetition of an important historical earthquake, and compare the losses incurred to each SC_k under this event with the corresponding cost of providing that level of seismic capacity.

A more robust procedure would be to consider all possible sources of ground motion at the site and to create a MDR exceedance curve, as has been presented in the previous section. Figure 2.2 shows the direct loss exceedance distribution curves which might be obtained from the MDR exceedance curves by assigning a nominal cost of 10,000 units to providing the SC_2 level of resistance and 12,000 units to providing that of SC_3. Additional losses such as those due to downtime for industrial and commercial activities and the impact this has on the regional economy could also be included in these curves.

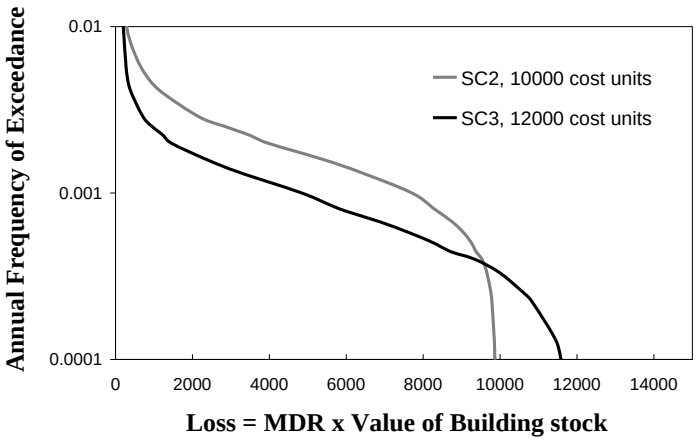

Figure 2.2 Loss exceedance probability curves for the acceptable levels of seismic resistance (taken from Figure 2.1) using a nominally assigned cost for each SCk, as indicated in the plot.

The annual average loss (*AAL*) is often used by the insurance and reinsurance industries to enable them to set annual premiums. The *AAL* is the expected value of a loss probability curve and can be thought of as the product of the loss for a given event *l* ($Loss_l$) with the annual probability of occurrence of event *l* (OP_l), summed over all events:

$$AAL = \sum_l (OP_l \cdot Loss_l) \tag{2.1}$$

This can be directly compared with the cost of implementing each SC_k in order to attain the optimum seismic capacity level. In Figure 2.2, the loss of SC_3 is higher than SC_2 at low probabilities of exceedance (corresponding to high levels of MDR) because the higher the value of the building stock, the higher the losses for a given MDR. However, for the same example the AAL of SC_2 is actually higher than SC_3.

Alternatively, the loss exceedance probability curves can be used to create total cost exceedance probability curves. These curves combine the cost of each SC_k with the direct cost of damage (i.e. loss). For a specified level of cost, the annual frequency of exceedance can be obtained from the plot for each SC_k and a decision can be made as to whether this probability is acceptable. The higher cost of the superior seismic resistance leads to higher total costs at low exceedance frequencies, when the majority of the building stock is predicted to be heavily or completely damaged. In addition, at high frequencies of exceedance when the MDR is low, the total cost of the more enhanced seismic capacity is greater. However, at intermediate annual probabilities of exceedance, the seismic resistance with the lowest total cost (i.e. the optimum SC_k) will depend on both the shape of the loss curve and the cost of the seismic resistance.

It is proposed herein to use a cost-benefit factor that is the sum of the initial construction investment (cost) and the average annual loss (or the average loss within a given time span) (benefit) as a basis for making a decision on whether the additional investment to achieve SC_3 as opposed to SC_2 is justified.

$$\text{C/B Factor} = \text{Cost}(SC_k) + \text{AAL}(SC_k) \quad (2.1)$$

As the levels of hazard will vary throughout the area of interest, not all locations will need to have the same level of SC_k, hence the SC_k with the lowest aforementioned cost/benefit factor should be assigned to each grid cell in the model.

2.4. Defining the Minimum Level of Seismic Resistance for Life Safety

In order to ascertain the minimum degree of seismic resistance required for each construction type, an uncomfortable but necessary decision must be taken by politicians, planners and code drafters regarding the tolerable levels of death, injury and persons rendered homeless as a result of an earthquake ground motion with a specified annual frequency of exceedance. This will not necessarily be stated as a single number of casualties for a single return period, but could be expressed as combinations such that a death toll of 1,000 could perhaps only be “tolerable” for a return period of, say, 100 years, whilst for a 10-year return period, the tolerable death toll could be limited to perhaps 50.

The number of fatalities can be taken as a proportion of the expected occupancy of the given construction type, and can be assumed to be controlled by the complete damage limit state (LS3). Therefore, the tolerable threshold can be reduced to a specific proportion of the exposed building stock reaching and exceeding LS3. Hence, once the most cost-effective SCk has been assigned to each location within the area under consideration, it should be checked to see if higher exceedance frequencies/probabilities than allowed at the threshold damage level are estimated; if so, the SC_k should be replaced with the next most cost-effective SC_k that meets the threshold.

The minimum level of required resistance and consequent investment in the building stock can thus be defined. The same procedure could also be applied to impose any number of risk criteria that will exclude any SC_k that violates the condition: limiting the proportion of buildings failing the extensive damage limit state (LS2) for specified return periods could effectively control both injuries and homelessness, and if applied to industrial and commercial buildings could also, in a crude manner, control downtime due to disruption.

2.5. Optimal Design Levels.

The outcome of these analyses will be an optimal map of SC_k levels. This now entirely circumvents the need to present seismic actions in the design code: the code need only present a zonation map, such as in Figure 2.3, and specify the corresponding design level to be applied in each zone. These design levels will be specified essentially in terms of the required levels of stiffness, strength and ductility capacity in buildings. There is thus no requirement to present a simplified response spectrum to represent the earthquake actions in the code and much less is there a requirement to anchor this spectrum to an arbitrarily selected return period.

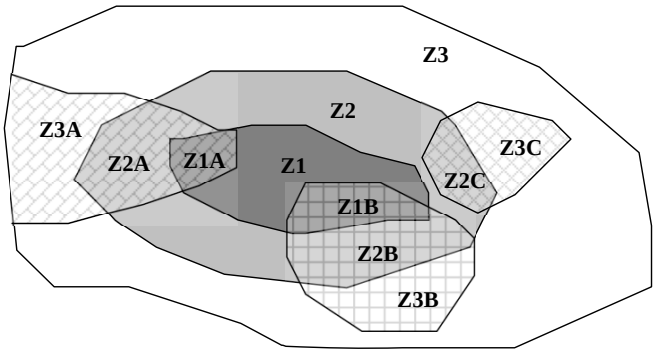

Figure 2.3 Schematic illustration of a design level zonation map, where each zone Z corresponds to a different SC_k.

3. CASE STUDY APPLICATION OF CALIBRATION METHOD

3.1. Case Study Area.

The calibration method presented in Chapter 2 has been applied to the northwest area of Turkey. This choice was due to two main reasons: the availability of a reliable PSHA input model and the fact that this region comprises zones which range from low to high seismicity. A building class of mid-rise reinforced concrete buildings has been considered for this illustrative example. All analyses presented herein have been done with the OpenQuake software (http://openquake.org), that is currently under open source development as part of the Global Earthquake Model initiative (www.globalquakemodel.org). Further details are provided in the OpenQuake Book (available from http://openquake.org).

The seismic hazard input data utilized herein comes from a preliminary seismic hazard model developed for Turkey (Demicioglu *et al.*, 2008). The PSHA model consists of a seismic source model based on two source typologies: area and faults. Faults are utilized to model large magnitude events (i.e. with moment magnitude $M_w \geq 6.7$), while area sources describe distributed seismicity for Mw ≥ 5.0. Area sources are employed for two different purposes: to model large-scale background seismicity ($5.0 \leq M_w \leq 6.5$), as well as seismicity around faults (that is, events not occurring on the fault plane but within its neighbourhood). Earthquake ruptures inside area sources are modeled as points, while on fault sources ruptures are modelled as rectangles, whose dimension (length and width) are derived from the Wells and Coppersmith (1994) magnitude-area scaling relationship. Figure 3.1 and Figure 3.2 depict the fault and area-based source models in terms of maximum moment magnitude.

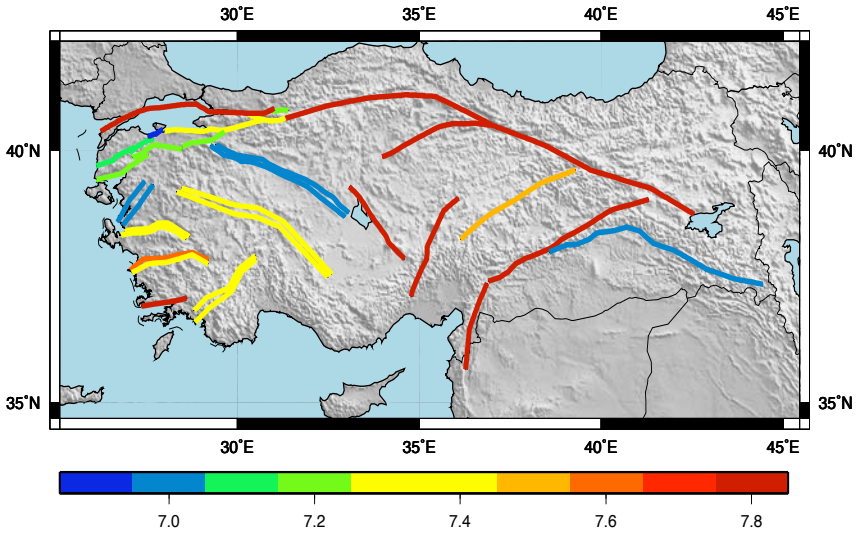

Figure 3.1 Fault source model for Turkey. Faults are assumed to be vertical, so only fault traces are shown. Colours represent maximum magnitude (M_w).

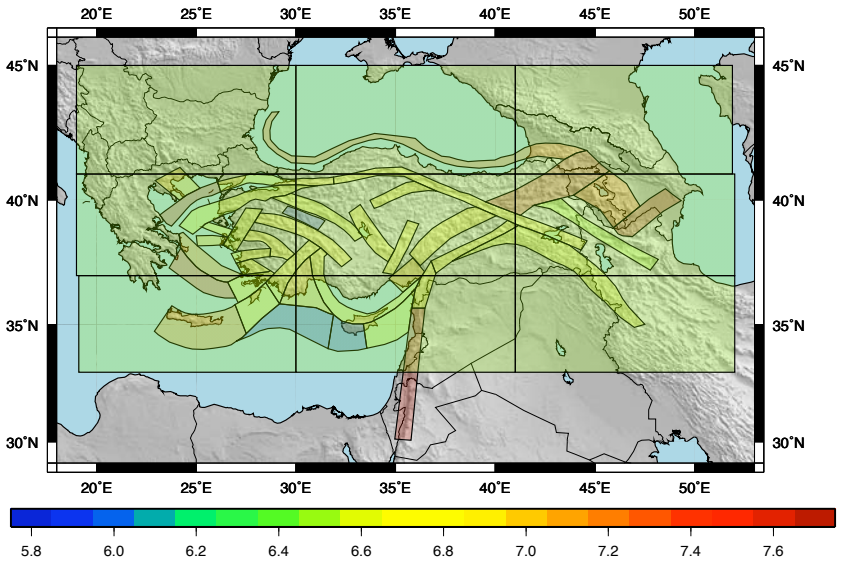

Figure 3.2 Area source model for Turkey. Large-scale rectangular background sources cover the entire country, whilst most of the small-scale area sources follow fault source geometries (colours represent maximum magnitude (M_w) in each source).

Faults are assumed to be vertical (dip angle equal to 90 degrees) with a strike-slip mechanism (rake angle equal to 0 degrees according to the Aki and Richards convention). Fault surfaces extend from 0 to 15 km depth. Area sources are associated to an average hypocentral depth of 3 km. Both faults and area sources occurrence rates follow a truncated Gutenberg-Richter magnitude frequency distribution.

The methodology described in Appendix A1 has been applied with the aforementioned PSHA model to calculate stochastic event sets and associated ground-motion fields for the purpose of the case study application.

3.2. Vulnerability Functions for Varying Design Levels (SC_k).

Three levels of design have been considered in this case study:

- Basic seismic design (SC_1);
- First level of improved seismic design (SC_2);
- Second level of improved seismic design (SC_3).

The first task of this study was to derive fragility curves for three different building designs with increasing seismic capacity. These fragility functions were derived using the DBELA fragility function approach (see Section A2.4) using the parameters and assumptions presented in Table 3.1 and Table 3.2. As can be seen from Table 3.2 the improved design levels lead to an increase in both stiffness and ductility. Such changes caused a slight decrease in the displacement demand and a considerable increase in the capacity, which consequently reduced the overall likelihood of suffering heavy damage or collapse.

Table 3.1 Material and geometric properties of the base building design (SC_1).

Parameters		Mean	COV	A	B	Distribution
H_{eff}/H_T	C – Sway	0.5	-	-	-	Deterministic
	B – Sway	[0.64] for n≤4 , [0.64-0.0125(n-4)] for n>4				Deterministic
f_y (MPa)		470	0.16	-	-	T. Normal
ε_c (LS2)		0.0035	0.51	-	-	Lognormal
ε_c (LS3)		0.0075	0.51	-	-	Lognormal
ε_s (LS2)		0.015	0.25	-	-	Normal
ε_s (LS3)		0.035	0.25	-	-	Normal
hs		2.84	0.03	2.50	3.30	T. Lognormal
lb		3.37	0.38	1.0	7.5	T. Lognormal
hb		0.48	0.14	0.3	0.6	T. Normal
h_c		0.49	0.28	0.4	1.2	T. Lognormal
h_{gm}/h_s (Emergent)		1.23	0.14	1.05	1.55	T. Lognormal

Table 3.2 Assumptions on stiffness and ductility.

Building design	Period/height relationship	Increase in ductility
SC_1	0.080H	0%
SC_2	0.075H	40%
SC_3	0.070H	80%

The fragility functions were combined with consequence functions in terms of economic losses (Bal *et al*. 2008) and fatalities (Spence *et al*., 2007) to produce vulnerability functions. Figure 3.3 and Figure 3.4 present the resulting vulnerability models for economic losses (as a ratio of the repair cost versus the replacement cost) and human losses (as the ratio of number of casualties to the total building occupants), respectively.

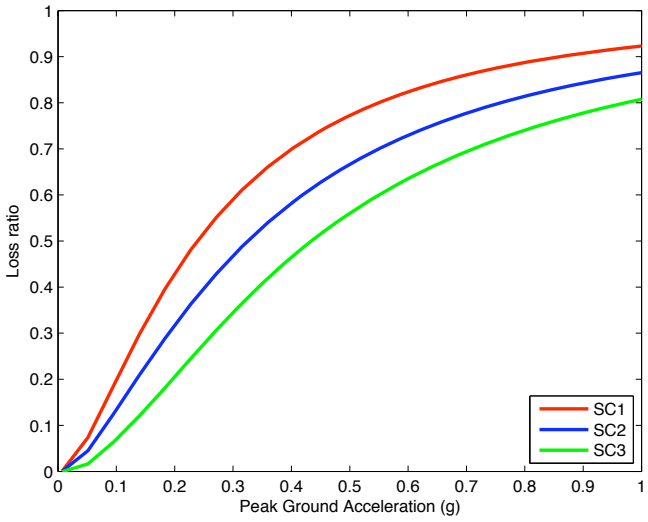

Figure 3.3 Economic vulnerability model.

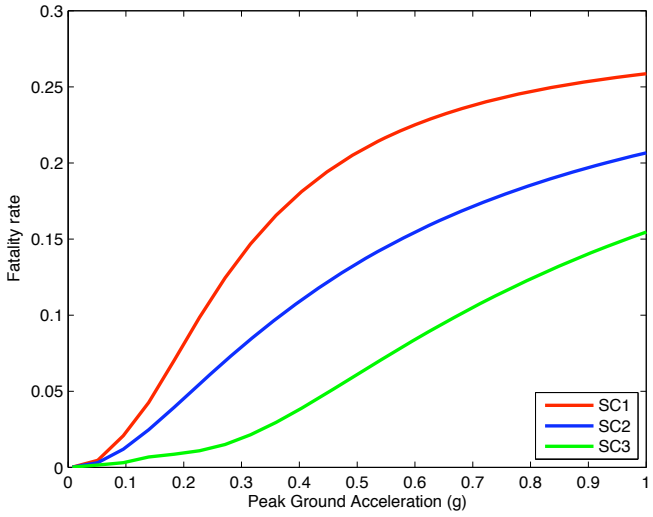

Figure 3.4 Fatality vulnerability model.

3.3. Loss Exceedance Curves for each SC_k.

In the first part of this exercise, only economic losses are considered. Using a probabilistic event-based risk calculator (as described in Appendix A1), a hundred realizations of the seismicity (each with a 50 years time span) were used, leading to about 3300 ground motion fields. Due to the small spatial resolution (0.05x0.05 decimal degrees which for this latitude represents a distance of about 4 km), it was possible to take into account the spatial correlation of the ground motion, using the Jayaram and Baker (2009) model. Figure 3.5 shows a hazard map in terms of PGA for a probability of exceedance of 10% in 50 years, which has been obtained from the ground motion fields.

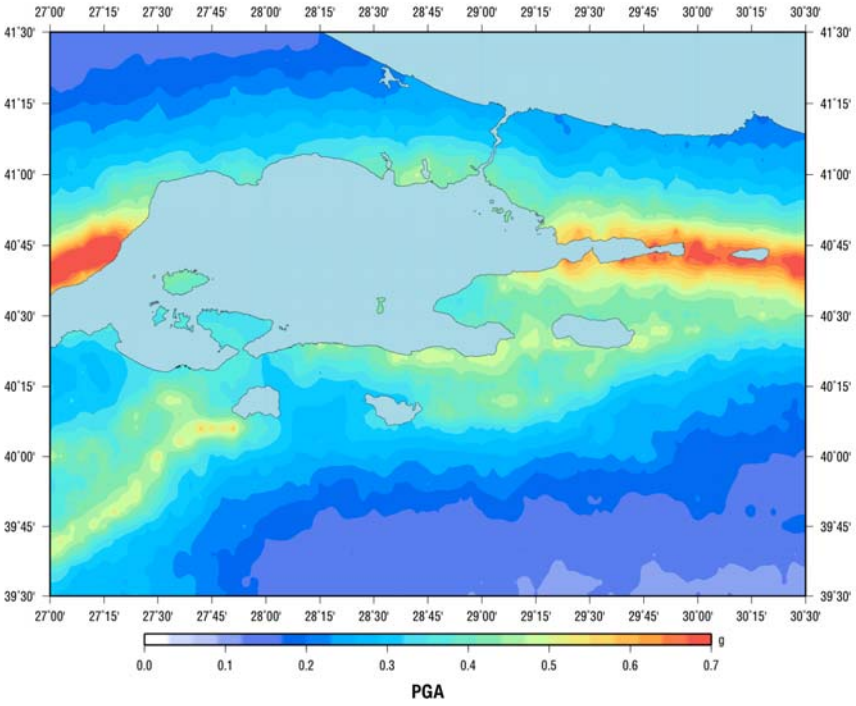

Figure 3.5 Hazard map for a probability of exceedance of 10 % in 50 years.

Once the seismic input was available, an aggregate loss exceedance curve was computed by placing a mid-rise reinforced concrete building in each location of the grid and following the methodology described in Appendix A1. Taking into account the aforementioned spatial resolution and excluding the areas where only water exists, a total of 2187 locations were considered. The same value of the building class was assumed in each grid cell, assuming that that probability of constructing in each grid cell is uniform; such assumption can be easily modified as a function of future land use planning. The base design level (SC_1) was assumed to be 1 in each grid cell, whilst SC_2 was assumed to cost 1.05 (i.e. 5% higher than SC_1) and SC_3 was assumed to cost 1.10 (i.e. 10% higher than SC_1).

Three separate analyses were carried out, each time assuming a uniform distribution of the building design level throughout the region of interest. The aggregate loss exceedance curves across the whole region for the three design levels are presented in Figure 3.6.

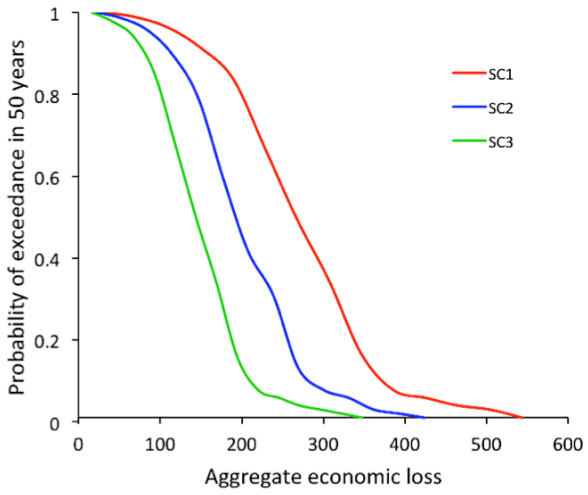

Figure 3.6 Aggregated curves assuming different seismic design levels.

3.4. Cost-Benefit Analysis for Optimum Design.

If only the aggregate loss exceedance curves were to be taken into account then the decision of which design level should be chosen would be straightforward: the most improved design (SC_3) produces lower economic losses. However, as discussed in Section 2.3, the initial cost to build such a seismic resistant structure should also be taken into account. Thus, for each location, a cost-benefit factor comprised of the initial cost plus the mean expected loss in 50 years was computed. A time span of 50 years was used as this is the commonly assumed design life of residential buildings. The latter value is derived by integration of each loss curve at each grid cell location. Again, these calculations were performed assuming the three different design levels (SC_1, SC_2, SC_3). As described in Section 2.3 the design level with the lowest cost-benefit factor was selected for each grid cell. Figure 3.7 shows the distribution of optimum design levels across the region of interest.

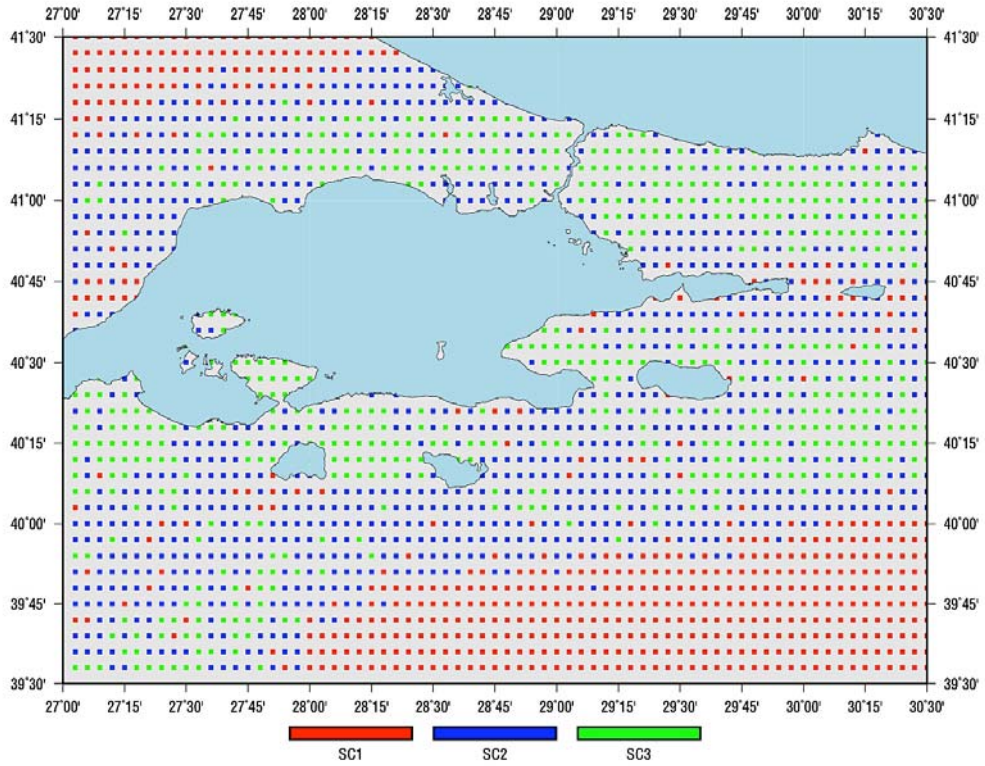

Figure 3.7 Optimized seismic design level distribution based on a cost-benefit analysis.

By comparing the distribution of building typologies with the hazard map presented previously in Figure 3.5, it can be concluded that in general for zones where medium to high ground motion values are expected, the usage of an improved seismic design is more economical, despite the fact that this typology has a higher initial cost. However, the regions of highest hazard lead to the lowest seismic design being the most cost effective as the losses are high regardless of the design level, and the combined cost-benefit factor is lowest for the most economical design. As expected, in regions where the seismicity is much lower, the minimum design level was the most cost effective. The base design (SC_1) provided the most economic solution in 29% of the sites whilst SC_2 and SC_3 proved to be the most profitable choice in 45% and 26%, respectively. The aggregate cost-benefit factor has been computed for the 4 scenarios (SC_1 in all cells, SC_2 in all cells, SC_3 in all cells and optimum SC_k for each cell) and as expected, the latter scenario (with the optimized distribution of design levels) proved to be the most cost-effective solution, as presented in Figure 3.8.

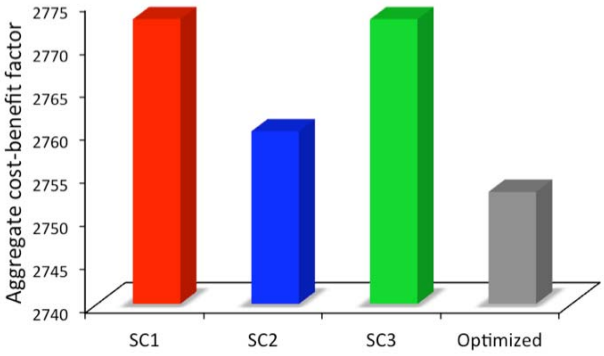

Figure 3.8 Aggregate cost-benefit factor for each design level distribution.

3.5. Minimum Level of Seismic Resistance for Life Safety

The results presented in Figure 3.7 do not take into account the performance of the buildings in terms of fatalities, which will have an influence on the minimum acceptable levels of design. A threshold on the number of casualties, for a certain return period, has been assigned for the purposes of this application. A loss curve was computed for the building class in each grid cell (using the vulnerability model presented in Figure 3.4), and the percentage of fatalities corresponding to a 2% probability of exceedance in 50 years (return period of 2475 years) was extracted and checked against an arbitrary and demonstrative "allowable" human loss of 10% of the occupants. A new distribution of design levels was created, assigning the building design that was closest to this threshold, but that did not exceed it, at each location. In the case where none of the design levels were complaint with this requirement, it was decided to attribute the safest typology, SC_3, for the purposes of this illustration. In real applications it would be necessary to use a much larger number of design levels and make sure that all design levels in the final design level map meet the threshold. It was also checked to see if a higher level of resistance than the one found for life safety would be more economically viable, based on the results in Figure 3.5, and if so, this was selected as the selected design level. Figure 3.9 presents the optimized design level distribution considering both life safety and cost effectiveness.

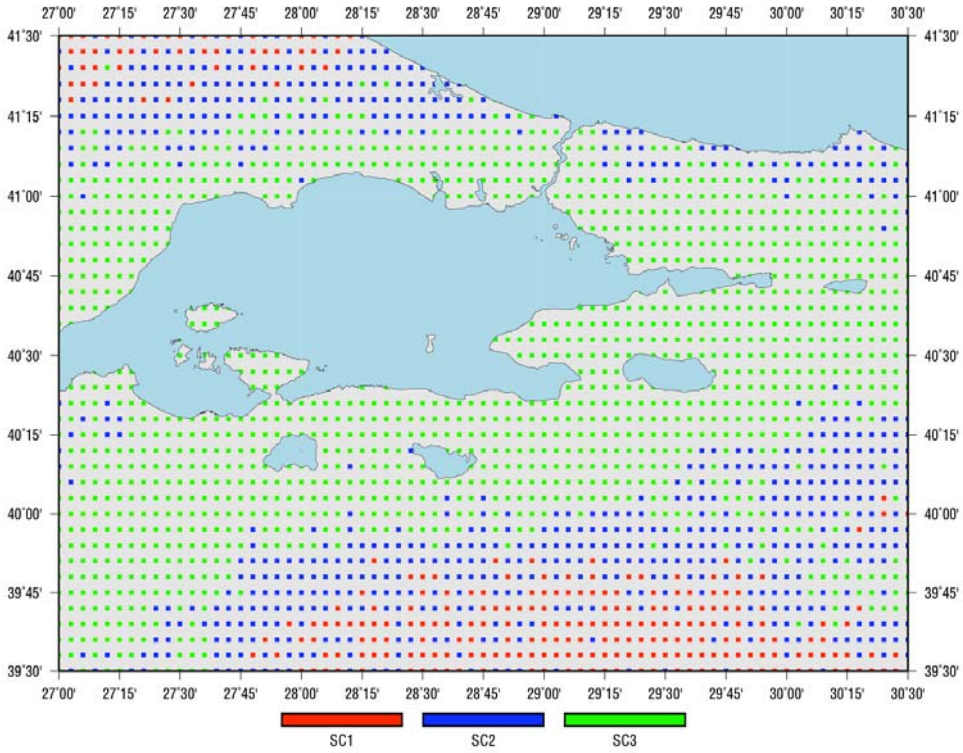

Figure 3.9 Optimized seismic design level distribution considering life safety and cost-effectiveness.

As can be seen from Figure 3.9, when considering human losses, the design level map is more conservative, with design level SC_3 being required in 62% of the locations while the design SC_2 was sufficient in 27% of the sites and the SC_1 only fulfilled the requirement in 11% of the sites. This optimized building distribution was used to compute the aggregate cost-benefit factor which was found to be 2764 units. Although this value is slightly greater than which was obtained when considering the optimized distribution based on cost-benefit analysis alone, it is important to note that it leads to a lower cost-benefit factor than that found considering any of the three design levels used alone throughout the area, as it is based on an optimal positioning of different levels of seismic design.

4. CONCLUSIONS

The procedures outlined in this deliverable represent a rather radical departure from the current format of seismic design codes. The purpose of a seismic design code could be stated as that of ensuring that minimum acceptable levels of seismic resistance are provided to the building stock, and this implicitly recognizes that most seismic design is carried out by engineers without specialist training in earthquake engineering. In current codes this is achieved through simplification (and consequent approximation) of the expected earthquake actions, anchored to arbitrarily selected return periods, and the specification of performance criteria to be met under these design loads. The natural choice for the adaptation of current codes to the PBSD framework is to specify two or more loading-performance couples, but this would generally mean perpetuating the shortcomings in the derivation of single limit state codes. The philosophy behind the procedure proposed herein is that the experts in engineering seismology and structural earthquake engineering charged with drafting the code should do more of the work outside the code, making the best use of their hazards models and their analytical tools, and only pass on to the engineer in the design office the outcome of these calculations.

An important qualification on the procedure outlined herein is that it corresponds to the minimum level of earthquake resistance, what is referred to as the basic objective in the Vision 2000 document [SEAOC, 1995]. In the terminology of current seismic design codes, this would correspond to buildings defined by normal occupancy or low importance factors, i.e. mainly dwellings. For higher occupancy buildings (e.g. schools), hazardous facilities or essential buildings (e.g. hospitals, fire stations), the design levels would clearly need to be increased within each zone. This is analogous to the coupling of the same performance levels to higher levels of ground motion envisaged in the famous Vision 2000 matrix (Figure 1.1).

These higher design levels could be obtained in a similar way, primarily by the application of exclusion criteria whereby the buildings in these categories would not be permitted to exceed limit state LS1 or LS2 for a given return period. This could alternatively, or additionally, be specified in terms of a minimum return period at which any such buildings would be expected to exceed one of these lower limit states.

The fact that the proposed procedures distil the hazard, exposure, vulnerability and cost components of the risk equation into a simple zonation map and a suite of design levels specified by combinations of stiffness/ductility, does not mean that it is necessarily desirable to remove information regarding the seismic hazard from the code. The proposed approach of specifying minimum levels of stiffness and ductility is likely to be applicable only to standard building types. Many engineers using the code will have a very good appreciation of the concepts and procedures of seismic design and the code should enable them to carry out checks and enhancements based on expected ground motions and appropriate dynamic analysis of the structure. The question then

arises of how these motions should be defined without making recourse to the arbitrary selection of return periods. Alternative formats for presenting earthquake actions in seismic design codes are discussed by Bommer and Pinho (2005) and a thorough description of this issue is provided in SHARE Deliverable 2.2 (Weatherill *et al.*, 2010), but it would be feasible to adopt the current approach of defining spectra through one or more mapped parameters, if however these parameters were obtained through disaggregation of the modelled losses that underlay the calibration of the design levels specified. Clearly, an important change from current code formats for compatibility with the framework proposed herein is to move from force-based design using acceleration spectra to displacement-based approaches, which is another important aspect being investigated in SHARE.

REFERENCES

Abo Al Ezz, A. (2007), Deformation and strength based assessment of seismic failure mechanisms for existing RC frame buildings, *MSc Dissertation*, ROSE School, IUSS Pavia, Italy.

Akkar, S., Sucuoglu, H., and Yakut, A. (2005) "Displacement-based fragility functions for low- and mid-rise ordinary concrete buildings", *Earthquake Spectra* 21(4), 901-927.

Allen, T. I., Wald, D. J., Hotovec, A. J., Lin, K., Earle, P. S. and Marano, K. D. (2008). An Atlas of ShakeMaps for selected global earthquakes. U.S. Geological Survey Open-File Report 2008-1236, 47 p.

ATC (1978), Tentative Provisions for the development of seismic design regulations of buildings - Report ATC 3-06, Applied Technology Council.

Bal, İ.E. (2005), Rapid assessment techniques for collapse vulnerability of reinforced concrete buildings, *MSc Dissertation*, İstanbul Technical University, Civil Engineering Department (in Turkish).

Bal, I. E., Crowley, H. and Pinho, R. (2008) "Displacement-Based Earthquake Loss Assessment for an Earthquake Scenario in Istanbul", *Journal of Earthquake Engineering*, 12: S2, 12 - 22.

Bal. I.E., Crowley, H. and Pinho, R. (2010), Displacement-based earthquake loss assessment: Method development and application to Turkish building stock, ROSE Research Report 2010/02, IUSS Press, Pavia, Italy.

Bommer, J. J., and Pinho, R. (2006) "Adapting earthquake actions in Eurocode 8 for performance-based seismic design," *Earthquake Engineering & Structural Dynamics*, 35(1), 39-55.

Bommer, J., Spence, R., Erdik, M., Tabuchi, S., Aydinoglu, N., Booth, E., Re, D. D., and Pterken, D. (2002). "Development of an Earthquake Loss Model for Turkish Catastrophe Insurance". *Journal of Seismology*, 6, 431–446.

Bommer, J. J., Pinho, R., and Crowley, H. (2005) "Using displacement-based earthquake loss assessment in the selection of seismic code design levels," in *Proceedings of the 9th International Conference on Structural Safety and Reliability*, Rome, Italy.

Bradley, B.A. (2010) "Epistemic Uncertainties in Component Fragility Functions," *Earthquake Spectra*, 26(1), 41-62.

Calvi, G. M. (1999). "A displacement-based approach for the vulnerability evaluation of classes of buildings". *Journal of Earthquake Engineering*, 26:1091–1112.

CEN - Comite Europeen de Normalisation (2003), Eurocode 8, Design of Structures for Earthquake Resistance – Part 1: General rules, seismic actions and rules for buildings, Pr- EN 1998-1. Final Draft, December 2003.

Chopra, A. K., and Goel, R. K., (2000) "Evaluation of NSP to estimate seismic deformation: SDF systems," *Journal of Structural Engineering*, 126(4), 482–490.

Crowley, H. and Pinho, R. (2004) "Period-height relationship for existing European reinforced concrete buildings," *Journal of Earthquake Engineering* 8(special issue 1), 93–119

Crowley, H., Pinho, R., and Bommer, J. (2004). "A probabilistic displacement-based vulnerability assessment procedure for earthquake loss estimation". *Bulletin of Earthquake Engineering*, 2:173–219.

Crowley, H., Pinho, R., Bommer, J., and Bird, J. (2006), Development of a Displacement-based Method for Earthquake Loss Assessment, ROSE Research Report 2006/01, IUSS Press, Pavia, Italy.

Crowley, H., Bommer, J.J. and Stafford, P. (2008) "Recent developments in the treatment of ground-motion variability in earthquake loss models," *Journal of Earthquake Engineering*, Special Issue, Volume 12, Issue S2, pp. 71-80.

Demircioglu, M.B., K. Sesetyan, E. Durukal and M. Erdik (2007). "Assessment of Earthquake Hazard in Turkey" *Proceedings of the 4th International Conference on Earthquake Geotechnical Engineering*, June 2007,Thessaloniki, Greece.

Dumova-Jovanoska, E. (2004). "Fragility Curves for RC Structures in Skopje Region", *Proceedings of the 13th World Conference on Earthquake Engineering*, Vancouver, Canada, Paper No. 3 (on CD).

Erberik, M., A. (2008) "Fragility-based assessment of typical mid-rise and low-rise RC buildings in Turkey" *Engineering Structures* 30(5), 1360-1374.

FEMA (2000), FEMA 310 - Handbook for the Seismic Evaluation of Buildings – A Prestandard, Federal Emergency Management Agency, Washington DC, USA.

FEMA (2003) HAZUS-MH Technical Manual, Federal Emergency Management Agency, Washington D.C.

Glaister, S. and Pinho, R. (2003) "Development of a simplified deformation based method for seismic vulnerability assessment". *Journal of Earthquake Engineering*, 7:107–140.

Jayaram, N. and Baker, J. W. (2009) "Correlation model for spatially distributed ground-motion intensities", *Earthquake Engineering and Structural Dynamics* 38(15), 1687-1708

Lang, K. (2002) Seismic Vulnerability of Existing Buildings, *PhD Thesis*, Swiss Federal Institute for Technology.

Luco, N., Ellingwood, B., R., Hamburger, R. O., Hooper, J. D., Kimball, J. K., and Kircher, C. A. (2007), "Risk-targeted versus current seismic design maps for the conterminous United States," *in Proceedings of the 2007 Convention of the Structural Engineers Association of California* (SEAOC)

Martinez, W. L. and Martinez, A. R. (2002).Computational statistics handbook with Matlab. Chapman & Hall/CRC, New York, USA.

NEHRP (2003), NEHRP Recommended Provisions for Seismic Regulations for New Buildings and Other Structures - Part I Provisions. Federal Emergency Management Authority.

Newmark, N.M. (1959) "A method of computation for structural dynamics". *Journal of the Engineering Mechanics Division*, ASCE, Vol. 85, No. EM3, pp. 67-94.

NZNSEE (2002), New Zealand national society for earthquake engineering: The assessment and improvement of the structural performance of earthquake risk buildings, draft prepared for the NZ Building Industry Authority.

Paulay, T., Priestley, M.J.N. (1992), Seismic Design of Reinforced Concrete and Masonry Buildings," John Wiley and Sons, Inc., New York.

Pinho, R., Bommer, J.J. and Glaister, S. (2002) "A simplified approach to displacement-based earthquake loss estimation analysis," *In Proceedings of the 12th European Conference on Earthquake Engineering*, London, England, Paper no. 738.

Porter, K. (2003), "An overview of PEER's performance-based earthquake engineering methodology," *Ninth Conference on Application of Statistics and Probability in Civil Engineering*; Proceedings. San Francisco, 2003.

Priestley, M. J. N. (1997), "Displacement-based seismic assessment of reinforced concrete buildings," *Journal of Earthquake Engineering*, (1)1, pp.157-192.

Priestley, M.J.N. (1998), "Brief comments on elastic flexibility of reinforced concrete frames and significance to seismic design," *Bulletin of the New Zealand National Society of Earthquake Engineering*, 31(4), 246-259.

Priestley M.J.N. (2003), Myths and fallacies in earthquake engineering, revisited, The Mallet Milne Lecture, IUSS Press, Pavia.

Priestley M.J.N., G. M. Calvi and M. J. Kowalsky (2007), Displacement-based seismic design of structures, IUSS Press, Pavia, Italy.

Rossetto, T. and Elnashai, A. (2005) “A new analytical procedure for the derivation of displacement-based vulnerability curves for populations of RC structures”. *Engineering Structures* 27(3), 397-409.

Rossetto, T. and Elnashai, A. (2003). “Derivation of vulnerability functions for European-type RC structures based on observational data”. *Engineering Structures* 25(10), 1241-1263.

SEAOC (1995), Vision 2000: Performance Based Seismic Engineering of Buildings. Structural Engineers Association of California, Sacramento, CA.

Shibata, A., and M. Sözen (1976), “Substitute structure method for seismic design in reinforced concrete,” *ASCE Journal of Structural Engineering*, 102(1), pp.1-8.

Silva, V., Crowley, H., Pagani, M., Monelli, D., Pinho, R. (2011) “Development and application of OpenQuake, an open source seismic risk assessment software,” *Submitted to Earthquake Engineering and Structural Dynamics*.

Singhal A, Kiremidjian, S. (1997) “A method for earthquake motion–damage relationships with application to reinforced concrete frames”. NCEER report, NCEER-97-0008, State University of New York at Buffalo, USA.

Spence, R. Ed [2007] ‘‘Earthquake disaster scenario predictions and loss modelling for urban areas,’’ LESSLOSS Report 7, IUSS Press, Pavia, Italy.

SYNER-G, (2011). “Fragility functions for common RC building types in Europe”. Deliverable 3.1. Available from URL: http://www.vce.at/SYNER-G/.

Vacareanu, R., Radoi, R., Negulescu, C. and Aldea, A. (2004).“Seismic vulnerability of RC buildings in Bucharest, Romania”. *Proceedings of the 13th World Conference on Earthquake Engineering*, 2004.

Wasserman, L. (2004). All of Statistics: A Concise Course on Statistical Inference. Springer, New York, 442 pp.

Weatherill, G., Crowley, H. and Pinho, R. (2010) Report on seismic hazard definitions needed for structural design applications. SHARE Deliverable D2.2, Available from URL: www.share-eu.org.

Wells, D. L. and Coppersmith, K.J., (1994) “New empirical relationships among magnitude, rupture length, rupture width, rupture area, and surface displacement”. *Bulletin of Seismological Society of America* 84, pp. 974–1002.

Yang, Y. (2009) “SDOF Characterisation of capacity-designed ductile RC frames for displacement-based assessment,” *MSc Dissertation*, ROSE School, IUSS Pavia, Italy.

A1. EVENT-BASED SEISMIC RISK ASSESSMENT

The methodology presented in Chapter 2 has used an event-based seismic hazard and risk assessment. The software OpenQuake (http://openquake.org) has been used for the calculations presented herein, and the methodology used for the risk assessment is outlined below. Further information is available in the OpenQuake Book, available from the aforementioned website.

This calculation workflow computes the probability of losses and loss statistics for a collection of assets, based on the probabilistic hazard. The losses are calculated with an event-based approach, such that the simultaneous losses to a set of assets can be calculated.

This workflow requires a number of calculators in order to calculate ground motion fields. Firstly, a Logic Tree Processor calculator uses information contained within the seismic source system together with a Monte Carlo approach to sample the logic tree structure and produce a seismic source model (SSM). Each seismic source model computed is used by the Earthquake Rupture Forecast (ERF) calculator to produce a list of all the possible ruptures occurring on all the sources in the SSM; each rupture is associated with a probability of occurrence in the time span specified by the user in the configuration file. Then, the Stochastic Event Set calculator uses the ERF to create one or several groups of ruptures. Each group represents a possible realization of the seismicity generated in the specified time span by the entire set of seismic sources included in the seismic source model. Afterwards, the Logic Tree Processor is again used to process the GMPEs system and provide the ground motion relationship that shall be used by the Ground Motion Field calculator, together with each earthquake rupture, to compute the ground motion values at a set of sites. During the generation of each ground motion field, the spatial correlation of the intra-event variability can be considered, so that assets located close to each other are likely to have similar ground motion levels (see e.g. Crowley *et al*., 2008 for a summary of ground motion variability treatment in loss models).

For each ground motion field, the intensity measure level at a given site is combined with a vulnerability function, from which a loss ratio is randomly sampled, for each asset contained in the exposure model, in the Probabilistic Event-Based Risk calculator. The loss ratios that are sampled for assets of a given taxonomy classification at different locations are considered to be either independent or fully correlated, knowing that the reality is likely to lie somewhere in between these two assumptions. The occurrence distribution of loss for a given asset is calculated using all of the ground motion fields, leading to a histogram of loss ratios which is then converted into a cumulative histogram, by calculating the number of cumulative occurrences for each interval of loss ratio. The rate of exceedance of each loss ratio is calculated by dividing the number of cumulative occurrences by the number of stochastic event sets multiplied by the length of each event set. By assuming a Poissionian distribution of the occurrence model, the probability of exceedance of each loss ratio is calculated. If an aggregated loss curve for a portfolio of assets is required, a secondary module is

used in order to aggregate the losses from all the assets in the exposure file, per event, before calculating the occurrence distribution of loss.

This approach can be used to compute a loss curve for each asset within the exposure model, or by aggregating all the losses throughout the region per ground motion field, an aggregated loss curve representative of the whole set of assets within the exposure file is obtained. The workflow in Figure A.1.1 describes this procedure.

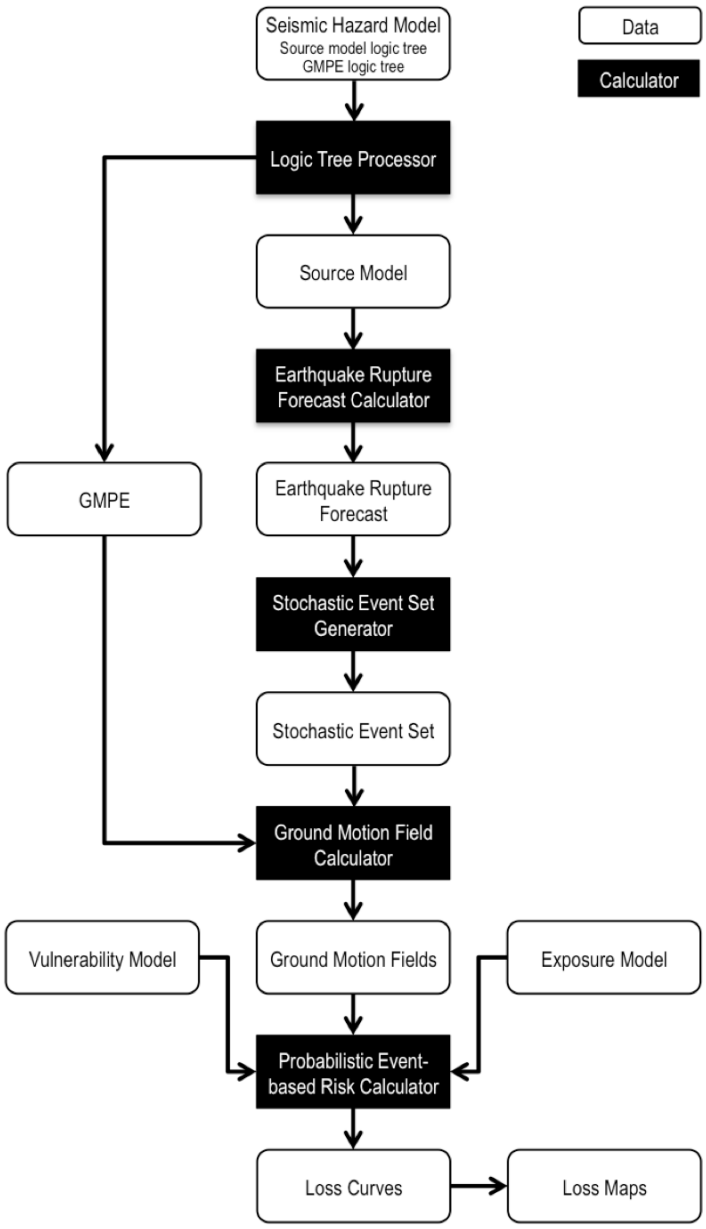

Figure A1.1 Workflow of Probabilistic Event-Based Risk calculator

A2. DISPLACEMENT-BASED EARTHQUAKE LOSS ASSESSMENT (DBELA)

A2.1. Introduction

DBELA is a methodology based on a proposal by Calvi (1999) and uses the concept of Direct Displacement Based Design (DDBD) devised by Priestley (1997). DBELA is used for assessing the capacity of structures and it is based on the deformation capacity of the elements that comprise them. Since it has been shown by some authors (Priestley, 2003) that damage in structures is directly related to strain of the constituent materials, and therefore to displacement, this methodology uses displacement in order to characterize the capacity of the structure and also as a means for the representation of the demand through displacement response spectra. The details of the methodology can be found in several consecutive studies (Pinho *et al*., 2002, Glaister and Pinho, 2003; Crowley *et al*., 2004; Crowley *et al*., 2006; Bal *et al*., 2010).

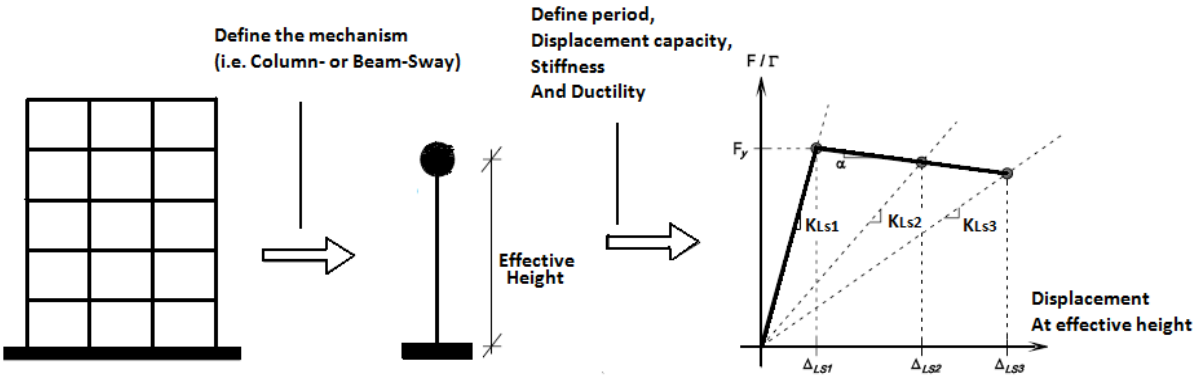

Figure A2.1 Displacement capacity of a structure modelled as a SDOF (Bal et al., 2010)

In this methodology different building classes are defined. This definition is based on the assumed response mechanism of the structure, either beam-sway or column-sway mechanism. Modern reinforced concrete buildings, designed according to modern capacity design principles, are often assumed to exhibit a beam-sway mechanism while buildings that do not have seismic resistant design can usually be assumed to exhibit a column-sway mechanism. However, since a building that has been designed for seismic loads can still exhibit a column sway mechanism and a building that has not been designed for seismic loads can still exhibit a beam sway mechanism, a sway potential index is used. The sway potential index used herein compares the strength/stiffness of the beams with the strength/stiffness of the columns.

In the displacement-based approach applied in the DBELA methodology, the substitute structure concept (Shibata and Sozen, 1976) is used along with the calculation of the effective period of vibration of the building at different damage limit states (Figure A2.1). The damping of the structure is considered by reducing the displacement response spectrum by a damping reduction

factor. This reduction factor depends on the equivalent viscous damping of the system which is a function of the system ductility for a given target displacement.

In order to apply the DBELA methodology, the definition of different building classes as a function of the response mechanism that is assumed is needed; that is, to characterize each structure as a building exhibiting a beam sway mechanism or a column sway mechanism by using the sway potential index.

The basic formulae for determining the displacement capacity at the centre of the seismic force for both beam sway and column sway mechanisms are shown as follows:

$$\Delta_{LS}^{bm-sway} = \theta_{by}\, k_1 H + \theta_{bp}\, k_1 H \tag{A2.1}$$

$$\Delta_{LS}^{cl-sway} = \theta_{cy}\, k_1 H + \theta_{cp}\, k_2 h_s \tag{A2.2}$$

where θ_{by} and θ_{cy} are the yield rotation capacities of beams and columns respectively; κ_1 is the effective height coefficient used to obtain the equivalent height of the deformed SDOF system; H is the height of the building; θ_{bp} and θ_{cp} are the plastic rotation capacities at a given post-yield limit state of beams and columns respectively; h_S is the ground floor story height; and κ_2 is 1 for reinforced concrete buildings.

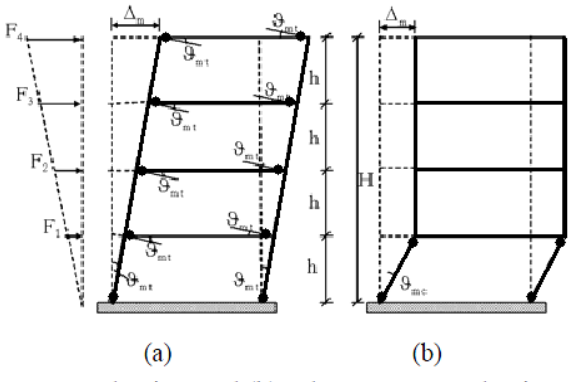

Figure A2.2 (a) Beam-sway mechanism and (b) Column-sway mechanism for RC frames

A2.2. Displacement Capacity Formulae

A2.2.1. Section Deformation Capacity

For reinforced concrete buildings, the calculation of the yield and plastic rotation capacities of the beams and columns for the two mechanisms is based on simple principles of mechanics related to the behaviour of reinforced concrete (RC) members.

As an introduction to the deformational behaviour of RC members, the yield displacement and plastic displacement capacity of a cantilever in simple bending will be presented using a RC cantilever column, as shown in Figure A2.3. It should be noted here that many of the assumptions and choices made in the derivation of the displacement capacity equations described in the

following passages (such as the effective height coefficient, the equation to calculate the plastic hinge coefficient, the empirical factors to account for shear and joint deformations, amongst others) can be easily adapted depending on the assumptions chosen by the user due to the flexible, transparent nature of the methodology.

A typical cross section of a column is shown in Figure A2.3a and the strain profile at that section is shown in Figure A2.3b. At any cross section, the curvature can be computed by the sum of steel and concrete strains (ε_s, and ε_c, respectively) at the two extremes of the section, divided by the effective depth, *d'*. The column member is presented in Figure A2.3c, with a height h_s. When the section at the base of the column reaches the yield curvature, $\emptyset_y$, the first limit state is reached and the curvature distribution with height can be conservatively approximated as triangular (Figure A2.3d). By integrating the curvature distribution along the length of the deformed member, the tangent yield rotation shown in Figure A2.3f, θ_{ty}, is obtained and the yield displacement at the top of the column can be computed by the moment-area method, as described in what follows.

Priestley (1998) first showed how the yield curvature, $\emptyset_y$, of reinforced concrete sections is independent of the strength, but rather dependent on the yield strain of the reinforcement steel and the geometry of the section, as shown in the following equations:

$$\emptyset_y = 1.7\frac{\varepsilon_y}{h_b}\ for\ beam\ sections \qquad \text{(A2.3)}$$

$$\emptyset_y = 2.14\frac{\varepsilon_y}{h_c}\ for\ column\ sections \qquad \text{(A2.4)}$$

where h_b is the height of the beam section, h_c is the depth of the column section and ε_y is the yield strain of the reinforcement steel.

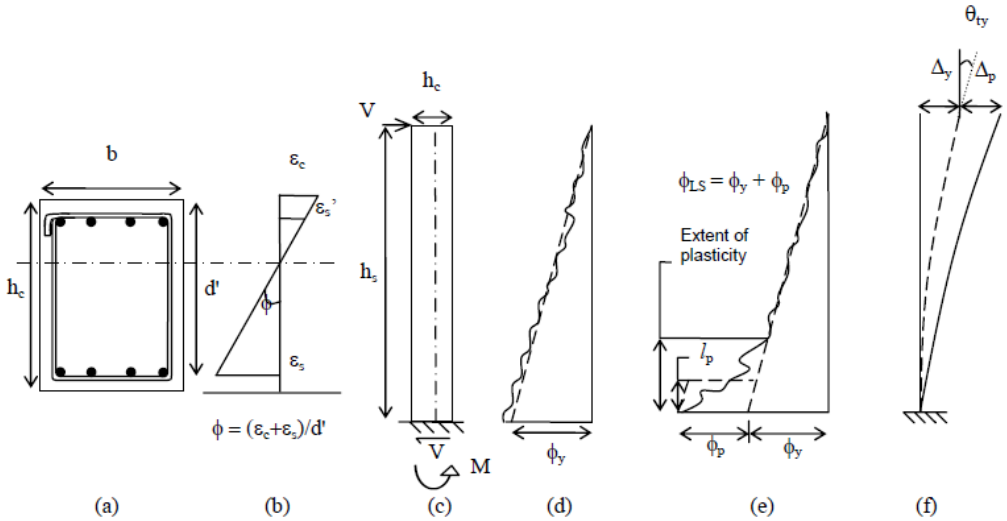

Figure A2.3 (a) typical poorly-confined reinforced concrete column section, (b) strain profile and definition of curvature, (c) prismatic reinforced concrete cantilever, (d) curvature distribution with height when the section at base reaches yield curvature (limit state 1), (e) curvature distribution with height at post-yield limit states, (f) components of total lateral tip deflection (modified from Paulay and Priestley 1992)

A2.2.2.Element Deformation Capacity

The tangent yield rotation at the top of the column, θ_{ty}, shown in Figure A2.3f, is calculated by integrating the curvature distribution at yield for a column (Equation A2.5) and then this is increased using empirical factors proposed by Priestley (2003) to account for shear and joint deformations (Equation A2.6).

$$\theta_{ty} = \emptyset_y \frac{h_s}{2} = 2.14 \frac{\varepsilon_y}{h_c} \frac{h_s}{2} = 1.07 \varepsilon_y \frac{h_s}{h_c} \tag{A2.5}$$

$$\theta_y = 1.35 \theta_{ty} = 1.44 \varepsilon_y \frac{h_s}{h_c} \tag{A2.6}$$

The moment-area method is then used to find the yield displacement capacity, Δ_y, at the top of the column:

$$\Delta_y = \theta_y \frac{2}{3} h_s = 0.96 \varepsilon_y \frac{h_s^2}{h_c} \tag{A2.7}$$

The curvature distribution of the column at the post-yield limit states is presented in Figure A2.3e. The plastic curvature, θ_p, can be found from the difference between the limit state curvature, θ_{LS}, and the yield curvature at the base of the section, as shown in the following equation.

$$\theta_p = \theta_{LS} - \theta_y \tag{A2.8}$$

The limit state curvature has been approximated by the sum of the limit state steel and concrete strains at the two extremes of the section ($\varepsilon_{s(LSi)}$ and $\varepsilon_{c(LSi)}$, respectively), divided by the total depth of the column section. The dotted lines in Figure A2.3e show the approximate curvature distribution that has been assumed in order to simplify the integration of the actual curvature profile. In this way, the plastic curvature may be multiplied by a plastic hinge length, l_p, assumed here to be half of the section depth (see Paulay and Priestley 1992), to give the plastic rotation capacity:

$$\theta_p = \emptyset_p l_p = \emptyset_p * 0.5 h_c \left(\varepsilon_{c(LSi)} + \varepsilon_{s(LSi)} - 2.14 \varepsilon_y\right) * 0.5 \tag{A2.9}$$

As can be noted from Figure A2.3e, the plastic hinge length does not represent the total extent of plasticity, but may be considered to be a representative equivalent/effective length used for obtaining in a simplified manner the correct rotation value. The plastic displacement at the tip of the cantilever shown in Figure A2.3f is then found by multiplying the plastic rotation by the height of the column:

$$\Delta_p = \theta_p h_s = \left(\varepsilon_{c(LSi)} + \varepsilon_{s(LSi)} - 2.14 \varepsilon_y\right) \ 0.5 h_s \tag{A2.10}$$

The total limit state displacement capacity given in Equation (A2.11) is finally obtained by adding the yield displacement, from Equation (A2.7), to the plastic displacement.

$$\Delta_{LSi} = \Delta_y + \Delta_p = 0.96 \varepsilon_y \frac{h_s^2}{h_c} + \left(\varepsilon_{c(LSi)} + \varepsilon_{s(LSi)} - 2.14 \varepsilon_y\right) 0.5 h_s \tag{A2.11}$$

In summary, Equation (A2.7) is used to define the capacity at the top of the column for Limit State 1 (yield) and Equation (A2.11) for Limit States 2 and 3 (post-yield), where the two post-yield states are distinguished by the specified allowable concrete and steel limit state strains.

A2.2.3.Structural Displacement Capacity

When beam-sway and column-sway RC frames need to be considered, the single-degree-of-freedom system has an assumed curvature distribution for both mechanisms that varies linearly with a zero value at the mid-span of the member (beam or column, respectively). Thus the beam and column yield curvatures presented in Equations (A2.3) and (A2.4) can be used in conjunction with the assumed curvature distributions, which are integrated to predict the yield chord rotation of either the beam-sway (θ_{by}) or the column-sway (θ_{cy}) frame mechanisms which are used in Equations (A2.1) and (A2.2), respectively, to calculate the yield displacement capacity at the centre of seismic force. The resulting yield displacement capacity (Δ_{LS1}) formulae for beam- and column-sway frames are presented in Equations (A2.12) and (A2.13) respectively; these are used to define the first structural limit state.

$$\Delta_{Sy}^{bm-sway} = 0.5 e f_h H_T \varepsilon_y \frac{l_b}{h_b} \tag{A2.12}$$

$$\Delta_{Sy}^{cl-sway} = 0.43 e f_h H_T \varepsilon_y \frac{h_s}{h_c} \tag{A2.13}$$

Post-yield displacement capacity formulae are obtained by adding a plastic displacement component to the yield displacement, the former being calculated by multiplying together the limit state plastic section curvature ($\emptyset_p$), the plastic hinge length (l_p), and the height/length of the yielding member. Thus, the limit state structural displacement capacity (Δ_{LSi}) for RC beam- and column-sway frames are obtained, as presented in Equations (A2.14) and (A2.15), respectively:

$$\Delta_{SLSi}^{bm-sway} = 0.5 e f_h H_T \varepsilon_y \frac{l_b}{h_b} + 0.5(\varepsilon_{C(LSi)} + \varepsilon_{S(LSi)} - 1.7\varepsilon_y) e f_h H_T \tag{A2.14}$$

$$\Delta_{SLSi}^{cl-sway} = 0.43 e f_h H_T \varepsilon_y \frac{h_s}{h_c} + 0.5(\varepsilon_{C(LSi)} + \varepsilon_{S(LSi)} - 2.14\varepsilon_y) h_S \tag{A2.15}$$

In this formulation, the soft-storey of the column-sway mechanism is assumed to form at the ground floor. Straightforward adaptation of the equations could easily be introduced in the cases where the soft-storey is expected to form at storeys other than the ground floor.

A2.2.4.Sway Potential Index

The sway mechanism of a certain building is controlled by capacity-design rules in existing modern codes. These rules are as follows:

i) Strong columns – weak beams
ii) Stiffness regularity between successive storeys (i.e. avoid a soft storey)
iii) Strength regularity between successive storeys (i.e. avoid a weak storey)

In most of the recent codes, the strong column-weak beam provision is satisfied by comparing the beam end moment capacities with column end moment capacities, including an uncertainty of 15-20% due to slab contribution and possible material strength variations.

The soft storey condition commonly occurs in buildings with open fronts at the ground floor or with particularly tall first storeys. Soft storeys are usually revealed by an abrupt change in interstorey drift. Basically, the columns which have the same section dimensions in successive floors must also have the same stiffness (essentially this means the same or similar storey heights) so that a certain floor does not develop significantly more drift than the others. Although a comparison of the stiffnesses in adjacent storeys is the direct approach, a simple first step might be to compare the interstorey drifts. According to FEMA (2000) and the New Zealand draft code (NZSEE, 2002), the stiffness of lateral force resisting system in any storey shall not be less than 70% of the stiffness in an adjacent storey above or below, or less than 80% of the average stiffness of the three storeys above or below. Eurocode 8 (CEN, 2003) specifies that there should not be significant difference in the lateral stiffness of individual storeys and at any storey; the maximum displacement in the direction of the seismic forces should not exceed the average storey displacement by more than 20%.

A weak storey irregularity occurs mostly in the absence of infill walls in a certain floor, which is often the first floor. The storey strength is the total strength of all the lateral force-resisting elements in a given storey for the direction under consideration. Weak storeys are usually found where vertical discontinuities exist, or where member size or reinforcement has been reduced. The result of a weak storey is a concentration of inelastic activity that may result in the partial or total collapse of the storey. According to FEMA (2000) and the New Zealand draft code (NZSEE, 2002), the strength of lateral force resisting system in any storey shall not be less than 80% of the strength in an adjacent storey, above or below.

The sway potential of a building is best defined by a pushover analysis, or better by an adaptive pushover analysis; nevertheless, some approximate prediction methods are available. The first prediction method, a strength-based index, has been proposed by Priestley *et al.* (2007) as described below in detail. Sway potential indices depending on the element dimensions, or consequently on element stiffness or deformation properties, have been proposed in different forms by several researchers. Bal (2005) proposed an index where the possibility of soft storey behaviour is predicted by using element moment of inertia values in the critical storey. Abo El Ezz (2007) has recently proposed a deformation-based index in which the sway potential of a certain floor is calculated by comparing the yield rotation capacities of beam and column members around a joint of a floor. The stiffness-based sway index, which is one of the main components of the DBELA methodology used in this study, is explained in detail below.

There are two different ways to arrive at the same formula of the deformation-based sway index. The first method relies on the observation that the sway index can be related to some general properties of the building. The probability of having a column-sway mechanism increases with:

i) increasing beam section depth
ii) decreasing column section depth
iii) increasing column length (storey height)

iv) decreasing beam length

If a higher sway index is assumed to represent a mechanism closer to column-sway, the expected index should then have the following basic form of:

$$R_i = \frac{h_b/L_b}{(h_c/L_c)} \tag{A2.16}$$

Where h_b and h_c are the beam and column section depths, respectively, whilst L_c and L_b are the column and beam lengths, respectively. The value of the index for i^{th} joint for a certain floor is:

$$R_i = \frac{h_{b,L}/L_{b,L}+h_{b,R}/L_{b,R}}{2(h_{c,B}/L_{c,B})} \tag{A2.17}$$

where sub-indices "L" and "R" refer to "Left" and "Right" and "B" refers "Below", respectively. The index per floor could then be obtained by averaging the result of Equation (A2.18) for each floor:

$$S_{def,j} = \frac{\sum_{i=1}^{n} R_{i,j}}{n} \tag{A2.18}$$

where "n" is the total number of joints at floor "j".

Another way to derive the same formula is the comparison of the yield rotational capacities of the members adjoining in the same structural joint of a certain floor, assuming that the rotation capacity is inversely proportional to the member stiffness and strength. The index is given by:

$$R_i = \frac{2\theta_{cy,B}}{\sum \theta_{Beams}} = \frac{2\theta_{cy,B}}{\theta_{by,L}+\theta_{by,R}} \tag{A2.19}$$

where $\theta_{cy,B}$ is the yield rotation of the column below the joint, $\theta_{by,L}$ is the yield rotation of the beam to the left of the joint, and $\theta_{by,R}$ is the yield rotation of the beam to the right of the joint. As given by Priestley *et al.* (2007), member rotation is a function of a constant, steel yield strain, member section depth and member length. It can be readily noted that the steel yield strains and constants would be cancelled, assuming that columns and beams are constructed with the same steel material. In this case, Equation (A2.19) leads to Equation (A2.18).

Regardless of the difference in storey heights, the deformation-based sway index is assumed to indicate a beam-sway mechanism below 1.00 and a column-sway mechanism above 1.20. Considering the fact that beams carry almost zero axial force, the column- sway limit is shifted to a little higher than 1.00 in order to represent the increase in column strength and stiffness due to axial forces on columns.

A2.3. Yield and Limit State Periods in DBELA

The yield period is the period of the representative single-degree-of-freedom system which would oscillate having the yield stiffness of the system. The so-called “yield stiffness” is the secant stiffness where the force at which the first limit state is reached is divided to the first limit state displacement.

A comprehensive study by Crowley and Pinho (2004) proposes the yield period of bare RC frames as:

$$Ty = 0.1\ H_n \tag{A2.20}$$

where H_n is the total height of the structure. Yang (2009) has revised this formula for capacity-designed ductile frames and suggested 0.075 to replace 0.10 in Equation (A2.20). The elongated period at any given limit state is then calculated as function of the ductility of that limit state, as given below:

$$T_{LS} = T_y \sqrt{\frac{\mu_{LS}}{1 + \alpha\mu_{LS} - \alpha}} \tag{A2.21}$$

A2.4. DBELA-Based Fragility Functions

The displacement capacity and period of vibration equations described in the previous section can be used to derive fragility functions. In this methodology, for each building in a randomly generated population of buildings, the displacement capacity and demand for three limit states needs to be calculated. The displacement capacity is calculated using simple formulae based on the material and geometrical properties of the buildings, and the period of vibration is calculated as a function of the height and ductility. Once these parameters are obtained, the displacement capacity of the first limit state is compared with the respective demand. If the demand exceeds the capacity, the next limit states need to be checked successively, until the demand no longer exceeds the capacity and the building damage state can be defined. If the demand also exceeds the capacity of the last limit state, the building is assumed to have collapsed. This procedure is schematically depicted in Figure A2.4 in which the capacity for each limit state is represented by Δ_i and the associated demand by S_{di}.

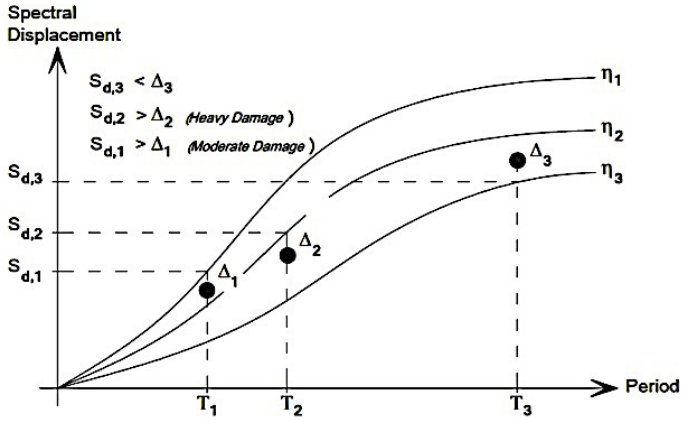

Figure A2.4 Comparison between the capacity for each limit state and the associated demand (Bal et al., 2010).

In this example, the demand exceeds the capacity in the first and second limit state but not in the third limit state, thus allocating the building to the third damage state. A full description of this methodology, in which the whole procedure is demonstrated step-by-step, can be found in Bal *et al*. (2010).

The DBELA method has been extended for the derivation of building fragility functions (Silva et al., 2011). The employment of analytical methods to create fragility functions has been widely used, mainly through the use of capacity spectrum methodologies (e.g. Vacareanu, 2004, Akkar et al., 2005, Rossetto and Elnashai, 2005, Erberik, 2008, amongst others). The methodology that is being proposed herein differs from the aforementioned ones because the method to calculate the non-linear response of the buildings is simplified and does not suffer from the convergence problems often experienced when using the capacity spectrum method with real accelerograms (e.g. Chopra and Goel, 2000).

This method relies on a Monte Carlo sampler to randomly create populations of buildings, based on a list of random variables of the structural properties defined in the capacity model. A detailed description of the required material and geometric characteristics in the DBELA methodology is presented in Section A2.2. The set of synthetic buildings is then passed to two distinct modules. One that computes the displacement capacity Δ_i based on the material and geometrical properties, and a second one, that calculates the displacement demand S_{di} for each limit state period using over-damped spectra at a level of equivalent viscous damping, representative of the combined elastic damping and hysteretic energy absorbed during the inelastic response, from a set of accelerograms. In order to compute the displacement spectrum from each ground motion record, a module that uses a Newmark integration process (Newmark, 1959) was developed. However, if a user wishes to avoid this additional computational effort, the displacement spectra can also be provided directly as an input to the calculator. The displacement demand for each limit state is then computed by modifying the elastic displacement spectrum by a correction factor ηi, representative of the equivalent viscous damping and limit state ductility. The selection of the set of accelerograms is a key parameter in this methodology and it should comprise a variety records, respecting the local seismic hazard properties

such as magnitude and peak ground acceleration range, most common fault failure mechanism, frequency content, duration or epicentral distance. This use of suites of accelerograms allows the consideration of the effect of the record-to-record variability of the seismic input. Currently there appear to be no formal guidelines for the selection of ground motion records to use in fragility curves generation. Many authors choose to gather sets of natural or synthetic records that are subsequently scaled to cover the range of ground motion levels that might occur in the region of interest (e.g. Dumova-Jovanoska, 2000, Singhal and Kiremidjian, 1997). However, this scaling process does not introduce changes in other properties of the records such as the frequency content or event duration, inherent to the magnitude of the event. The wide availability of strong motion databases (e.g.: ITACA [1] (Italy), K-Net/NIED [2] (Japan), ISMN [3] (Iran), GeoNet [4] (New Zealand), Daphne [5] (Turkey), ESD [6] (Europe), PEER [7] (global), COSMOS [8] (global)) should make the task of colleting a large number of natural accelerograms more easily achievable.

Once the capacity and demand displacements for the whole group of synthetic buildings are computed, a module is called to compare both sets of displacements, and thus allocate each building to a certain damage state. Thus, for each ground motion record, percentages of buildings in each damage state can be obtained and fragility curves can be extrapolated. In Figure A2.5, the building damage distributions for 4 records with different levels of spectral acceleration at a given period are presented. Then, the cumulative percentage is plotted against the associated intensity measure level, allowing the definition of a fragility curve for each limit state.

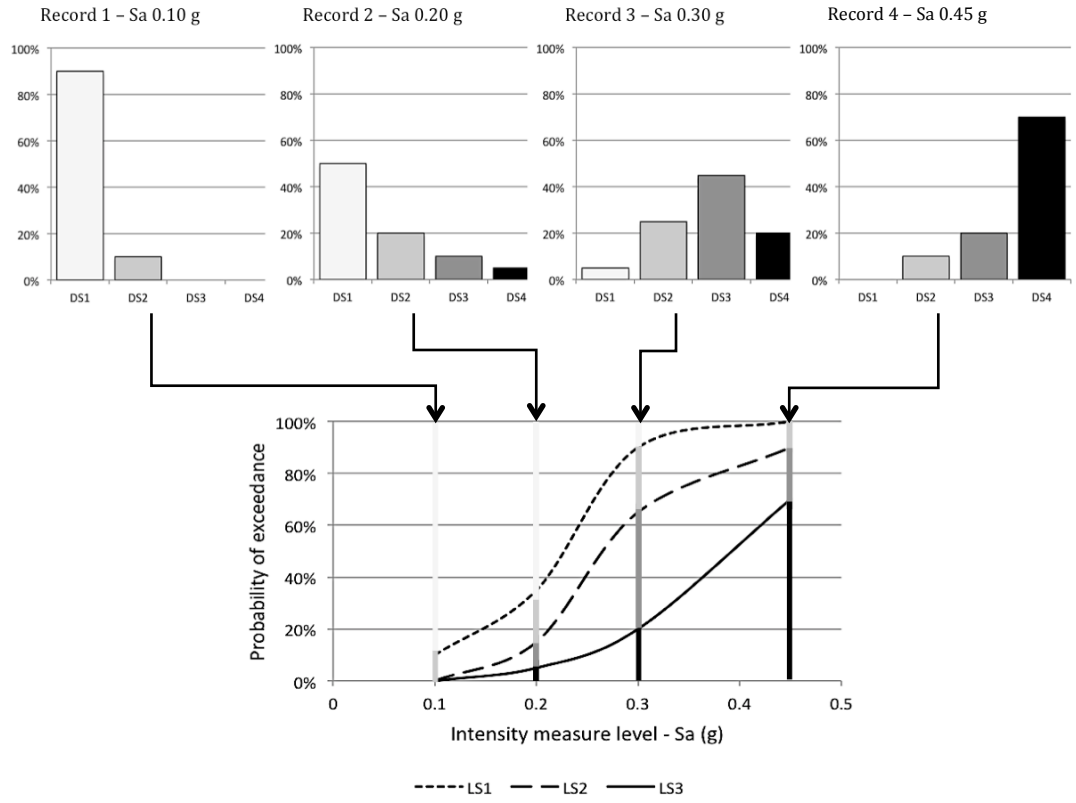

Figure A2.5 Derivation of fragility curves based on building damage distribution.

As can be inferred from Figure A2.5, the results for each ground motion record need to be associated with an intensity measure level. Within this methodology, it is possible to choose any intensity measure type to represent the record, as long as the necessary information is available. Macroseismic intensities such as MMI or EMS could be a natural choice since there is a direct relationship with the levels of damage in different building typologies. However, keeping track of the intensity at the location where the record was captured is not common and furthermore, macroseismic intensity does not take into account the influence of the frequency content on the structural response. Peak ground motion also shares this last shortcoming and even more importantly, it does not have a clear correlation with damage. The influence of the frequency content on the ground motion can be considered by choosing spectral acceleration or displacement to represent each record (Bommer *et al*., 2002). Other factors might play an important role in choosing the appropriate intensity measure type such as the availability of accurate GMPE or the possibility of taking advantage of existing seismic hazard data such as USGS ShakeMaps (Allen *et al*., 2008) on the risk calculations.

The fitting of a curve to the list of cumulative percentages versus intensity measure levels is done using the mean least squares method and assuming a lognormal distribution, which is the most common distribution to model fragility curves (SYNER-G, 2011). However, other distributions have been used in past vulnerability studies (e.g.: Lang, 2002; Rossetto and Elnashai, 2003) and for this reason, the definition of the probabilistic distribution should not be hard coded, and should be easily modified to other models. The logarithmic mean, λ, and logarithmic standard deviation, ζ, that are estimated for each curve will naturally have some uncertainty associated with them, due to the scatter of the results. Hence, a sampling method was implemented to properly evaluate the uncertainty on the statistics. This method consists in a continuous bootstrap sampling with replacement from the original dataset (Wasserman, 2004). For each dataset that is generated, the associated logarithmic mean and logarithmic standard deviation are estimated. This process is repeated N times, originating N different pairs of logarithmic mean and logarithmic standard deviation, whose distribution can be assumed as normal (Bradley, 2010). From these distributions, confidence intervals for different levels of confidence can be extracted. In Figure A2.6 a curve was fitted to some results and the sampling method was used to derive the distribution of the associated logarithmic mean and logarithmic standard deviation. According to Bradley (2010), 500 synthetic datasets are sufficient to achieve a satisfactory convergence on the results.

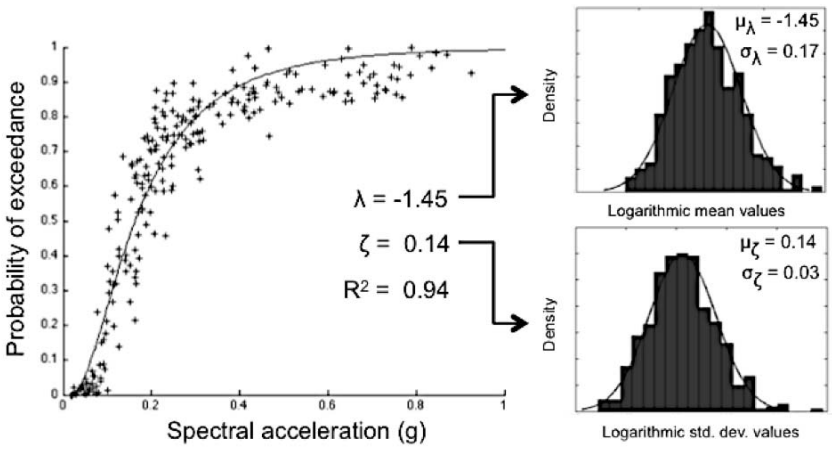

Figure A2.6 Statistical treatment of the parameters of the curve.

A2.5. Vulnerability Functions

This section presents how vulnerability functions can be produced using the fragility functions derived in the previous section together with consequence functions that relate damage to loss. In order to do so, for each intensity measure level an economic loss ratio needs to be computed, by multiplying the percentage of buildings in each damage state by the associated "damage ratio" (ratio of cost of repair to cost of replacement). The damage ratio per damage state varies significantly according to the building typology. As an example, Figure A2.7 presents the damage ratio per damage state for typical buildings in California (FEMA, 2003) and Turkey (Bal *et al*., 2008).

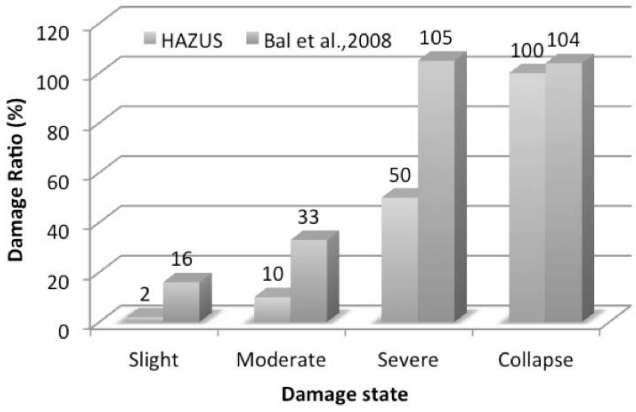

Figure A2.7 Damage ratios for reinforced concrete buildings, adapted from Bal et al. (2010).

The previously described methodology to derive vulnerability functions must be applied not only to the mean values of the parameters of each fragility curve, but rather to a set of randomly generated pairs of parameters (logarithmic mean and logarithmic standard deviation per fragility curve), allowing the propagation of this uncertainty to the vulnerability curves. This sampling process needs to be done taking into account the possible correlation between each parameter of the fragility curves. For example, if the correlation coefficient between two parameters is close to 1, then during

the sampling process if one of them is sampled to be above the mean, it is likely that the second one will also be sampled with a positive residual. On the other hand, if the pair of parameters has a coefficient of correlation close to 0, then the sampling process is done independently and the way one parameter is sampled does not affect the other one. As previously described, in the bootstrap methodology a list of logarithmic means and a list of logarithmic standard deviations are obtained for each limit state, making a total of six sets of parameters. The correlation coefficients are then computed by analysing the variation of each set of parameters with respect to the others. An example is presented below to better explain this relation. A set of fragility curves was computed for low-rise Turkish buildings and the bootstrap methodology was used to estimate the probabilistic distribution of the statistics of the three curves. In this process, 100 synthetic datasets were generated and for each dataset, the logarithmic mean and logarithmic standard deviation for each curve were computed. Then, the parameters associated to each dataset were plotted against each other; three of these plots with the respective correlation coefficient are presented in Figure A2.8.

The correlation between the parameters can be inferred by analysing the shape of the scatter. In the first combination, there is a thin dispersion of the data with a positive slope, which means that the values vary relatively linearly and proportionally. In other words, during the bootstrap method every time that a synthetic dataset led to a low mean for the first limit state, it also tended to produce a low mean for the second limit state, and vice-versa. In the second combination there is also a clear correlation between the two parameters but in this case it is negative, which means that the values tend to vary somewhat linearly but inversely. In the last combination, the scatter of the data is characterized by a wide dispersal and therefore, the correlation is not significant.

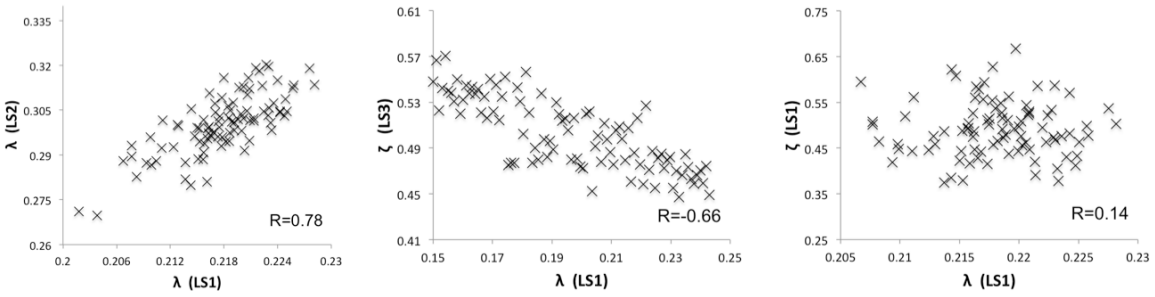

Figure A2.8 Correlation between the distribution parameters of the fragility curves.

Different approaches can be followed to randomly sample correlated normal distributions (e.g. Martinez and Martinez, 2002); a multivariate normal with Cholesky factorization of the covariance matrix approach is followed herein. This procedure can be described by the following expression:

$$X = ZR + \mu^T \tag{A2.22}$$

Where X represents the resulting n×d matrix with the randomly sampled parameters, Z represents a n×d matrix of standard normal random variable, R is a d×d upper triangular matrix obtained by

applying a Cholesky factorization to the covariance matrix, μ^T stands for a n×d matrix containing the mean of each distribution, n is equal to the number of required samples and d is equal to the number of normal distributions. In this case, d is equal to 6 (a logarithmic mean and a logarithmic standard deviation for each of the three limit state curves) and n should not be lower than 50.

Using the statistics from the previous example and the mean values of the damage ratios proposed by Bal *et al*. (2008), a set of 100 vulnerability curves was calculated. Then, for each intensity measure level, the distribution of the loss ratios was evaluated and a lognormal curve was fit to the data. In Figure A2.9 these results are presented, along with a histogram of the loss ratios and associated lognormal curve for a given spectral acceleration.

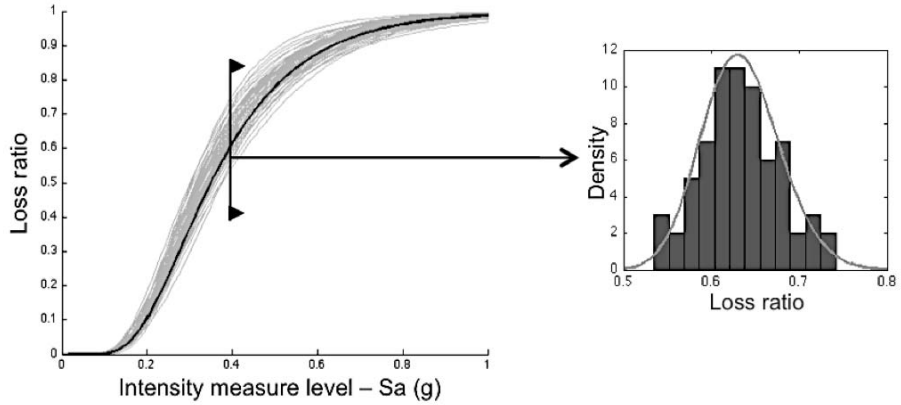

Figure A2.9 Vulnerability function and uncertainty per intensity measure level.

Thus, the final product of the vulnerability calculator is the probability distribution of loss ratio for each intensity measure level.